Deterministic vs. robust design optimization using DEM-based metamodels

Fransen, Marc P.; Langelaar, Matthijs; Schott, Dingena L.

DOI
10.1016/j.powtec.2023.118526

Publication date
2023

Document Version
Final published version

Published in
Powder Technology

Powder Technology 425 (2023) 118526

Contents lists available at ScienceDirect

Powder Technology

journal homepage: www.journals.elsevier.com/powder-technology

Deterministic vs. robust design optimization using DEM-based metamodels

Marc P. Fransen [a,*], Matthijs Langelaar [b], Dingena L. Schott [a]

[a] Department of Maritime and Transport Technology, TU Delft, the Netherlands
[b] Department of Precision and Microsystems Engineering, TU Delft, the Netherlands

HIGHLIGHTS

- We introduce robust optimization using DEM-based metamodels.
- Deterministic and robust metamodel-based design optimization (MBDO) are compared.
- The error of optimal designs is below 5% for verification and 10% for validation.
- The quality of MBDO highly relies on the quality of the metamodel and training data.
- Robust optimization leads to accurate mean performance and exhibits low variance.

GRAPHICAL ABSTRACT

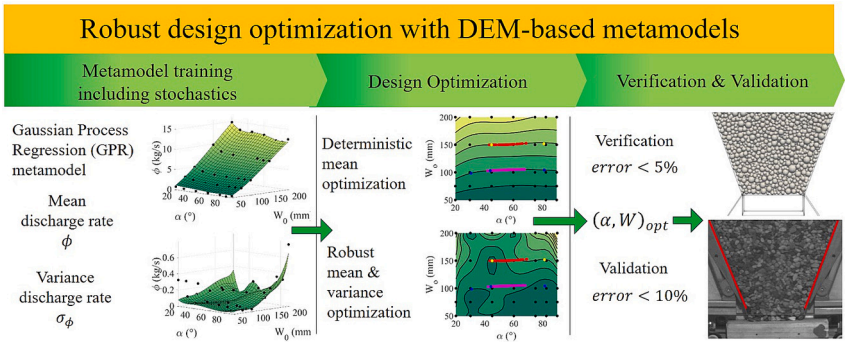

ARTICLE INFO

Keywords:
Robust optimization
Deterministic optimization
Metamodels
Optima validation

ABSTRACT

In design optimization of bulk handling equipment (BHE) we generally focus on the mean performance of the equipment. However, granular materials behave stochastic due to irregularities in particle shape and size which leads to stochastic performance of the equipment. To include the stochastic performance we propose robust metamodel-based design optimization (MBDO). The used metamodels are trained with stochastic performance data from randomly repeated discrete element method (DEM) simulations and predict mean and variance of the equipment performance. This method is compared to the conventional deterministic optimization method by means of a case study of a discharging hopper including verification and validation. The robust MBDO shows more distinctive optimal designs compared to the deterministic approach. In addition, the DEM-based metamodel is a relatively accurate method to predict DEM-model simulation results. However, the validation indicates that differences between DEM-model and experimental results highly affect the reliability of the found optima.

1. Introduction

In design of Bulk Handling Equipment (BHE) the use of Discrete Element Method (DEM) models to predict and evaluate performance in equipment design is increasing. The major advantage of this approach is the ability to evaluate a wide range of equipment designs without the need of conducting expensive experiments. The major downside is that if the number of particles [3], complexity of the equipment kinematics

* Corresponding author.
E-mail address: m.p.fransen@tudelft.nl (M.P. Fransen).

https://doi.org/10.1016/j.powtec.2023.118526
Received 11 November 2022; Received in revised form 12 March 2023; Accepted 4 April 2023
Available online 13 April 2023

[10,17], and interaction complexity [4,11] increases, the computation time of simulations increases as well. In addition, DEM models require calibration which also becomes a computationally intensive process if the number of calibration parameters is increased [2,5,7].

To counteract these high computational costs, metamodels are used in both calibration of and design of bulk handling equipment. Richter & Will introduced a metamodel-based global calibration (MBGC) framework and showed how metamodels can be effectively used in calibration [15]. Most DEM calibration optimization problems are multi-objective optimization problems (MOOP) with multiple calibration parameters [5]. Furthermore, a number of metamodeling approaches were successfully used in calibration of DEM models. Artificial neural networking (ANN), Gaussian process regression (GPR), multi-adaptive regression splines (MARS), and universal kriging (UK) were applied by Richter et al., [14]. An iterative Bayesian framework including a Gaussian mixture model (GMM) is used by Cheng et al., [2]. Based on the findings by Fransen et al. [7] it is recommended to use regression-based metamodels for the mean prediction to obtain accurate calibration results at low costs. Similar benefits are expected in using metamodels for design optimization where typically a large number of performance evaluations is required. However, it is important to note the limitations of the use of metamodels as they are approximations of the DEM model and therefore inherit a model error. Overall, metamodels perform well when used to interpolate but poor in extrapolation. Therefore, quality of the data and the sampling are important for the performance of a metamodel. Metamodel-based design optimization (MBDO) is referred to by Wang & Shan, [19] but in design of bulk handling equipment metamodels have not been used extensively [6]. In design, we generally have to deal with similar problems as in DEM model calibration: multiple design parameters and performance characteristics, which requires similar solving techniques.

Currently, the focus of optimization of BHE designs is on the mean performance of the equipment [8,17], i.e. the deterministic approach. However, granular systems are stochastic in nature resulting in uncertainty of design performance. To achieve an optimal design which has a good match to the mean performance and a minimized variance robust optimization strategies can be applied [9,12]. As indicated for the calibration of DEM models it is an effective approach to use DEM-based metamodels in MBDO instead of DEM simulations in the loop for calibration parameter estimation. In the case of robust design optimization, metamodels can be used in a similar fashion because they can predict both mean and variance. To the authors' knowledge, robust MBDO has not been investigated in relation to bulk handling equipment design.

The aim of this study is to show how robust metamodel-based design optimization can be applied to bulk handling equipment design with DEM-based metamodels and, to show how this method compares to a conventional deterministic approach and to identify application challenges. In this study, we present a methodology/framework for robust Metamodel-based Design Optimization (MBDO) for design of bulk handling equipment in Section 2. Next, Section 3 describes the design problem for a discharging hopper starting with a description of the experimental setup and DEM model, followed by the analysis of experimental and DEM results and sampling of the design space. It continues with a description of training the DEM-based metamodel and a formulation of the optimization problem. Lastly, the two design case studies are described to which the robust MBDO approach and deterministic MBDO are applied. In Section 4, the resulting DEM training set is evaluated as well as the resulting metamodel. This is followed by the results of the two design case studies where deterministic and robust optimization are compared. This section ends with a discussion on the obtained results related to the quality of the DEM data compared to experiments, mismatch between DEM metamodel predictions and the verification results, and the discrepancies observed between DEM metamodel predictions and experimental results.

2. Methodology

Bulk handling equipment is used to transport or process wide varieties of granular material. However, the behaviour of a granular material in general is stochastically distributed. This stochastic behaviour is caused by differences in particle packing's, sizes and in variations of material properties. Additionally, properties of the bulk material such as consolidation, moisture content, and temperature might affect the inter-particle physics leading to variable bulk strength and cohesion. This leads to distributed performance of the BHE around a certain mean performance. Even though this is known, the stochastic behaviour of the granular material and its effect on the equipment performance is not considered in the design process. Therefore, we introduce a methodology that includes the stochastic behaviour of granular materials in the bulk handling equipment design process.

In this section the global implementation of robust metamodel-based design optimization (MBDO) including verification and validation to design of bulk handling equipment is explained. The scheme in Fig. 1 shows the steps taken in the design process of BHE if MBDO, verification, and validation are included. A bulk handling equipment design problem starts with describing the system or problem where design and key performance indicators (KPIs) are defined. The next step in the approach is to create a numerical model of the equipment and the material that needs to be handled. For this purpose the Discrete Element Method (DEM) is used which can simulate behaviour of the bulk and interaction with the equipment. However, DEM models are generally a simplification of the physical system and are therefore reliant on calibration of material and contact parameters of the DEM model. After the calibration of the DEM model, this model needs to be validated to demonstrate that the model possesses a satisfactory range of accuracy consistent with the intended application of the model within its domain of applicability [16]. The calibrated and validated DEM model of a hopper used in this study is adopted from Fransen et al., [7]. DEM simulations take a considerable amount of time, which makes direct use of DEM models in

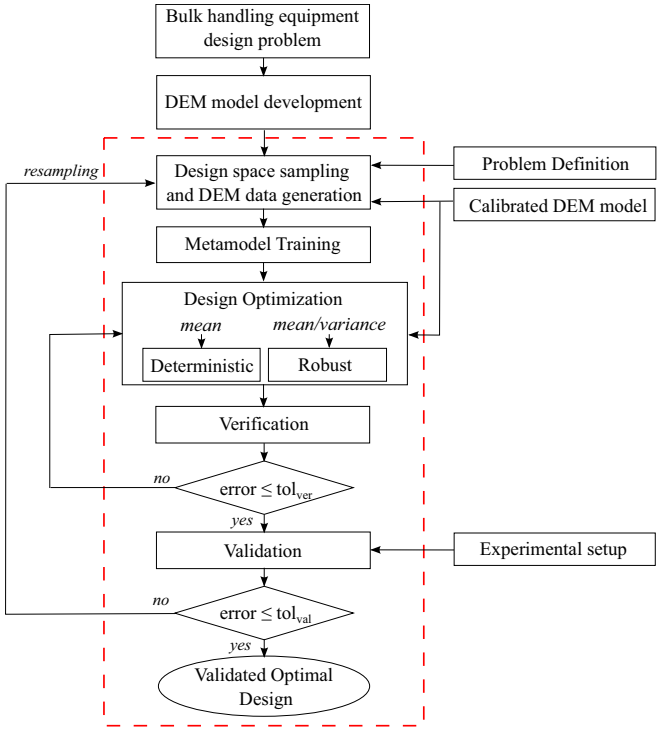

Fig. 1. Framework for Metamodel-based Design Optimization (MBDO) (red area) included in the process for bulk handling equipment design. (For interpretation of the references to colour in this figure legend, the reader is referred to the web version of this article.)

optimization inconvenient. To overcome this, a metamodel-based design optimization (MBDO) procedure can be used. This procedure uses a DEM data set to train a metamodel which gives predictions on BHE performance at low cost.

The first block in MBDO is *design space sampling and DEM data generation* shown in Fig. 1. After sampling the data, the DEM model can be used to generate the data. As the DEM model is stochastic due to the random initial packing of material this means that the simulations need to be repeated for each sampling point. This gives information about the average performance and the standard deviation of the design performance prediction. For a metamodel to be able to predict both mean and variance, it is essential that both are included in training the metamodel.

The second step in MBDO is *metamodel training*, which has been thoroughly described by Fransen et al. for a DEM case study [6]. For the proposed robust optimization it is required that information on the standard deviation of a KPI is supplied during training of the metamodel such that the metamodel can be trained to give predictions of both mean and variance of the KPI. In training the metamodel, hyper-parameter optimization is included such that the best fit of the metamodel to the data is obtained [13]. Moreover, a common step is to use resampling to improve the quality of the metamodel. However, when the set verification and validation tolerances are not violated by the initial sample resampling is not required. In Section 3.4 the metamodel training procedure and the relation to the case study is discussed in more detail.

After training the metamodel, the next step is *design optimization* which can be further divided in two types, deterministic and robust optimization. In deterministic optimization, only the mean performance of the BHE is used to find the optimal design whereas in robust optimization the standard deviation of the BHE performance is also included. These differences are further discussed in Section 3.5, which also elaborates, on solving the optimization problem leading to the optimal design(s). Next, the found optima need to be verified by carrying out DEM simulations of the found designs. For the *verification* of the results, a tolerance is set for the maximum error of the designs' performance relative to the optimization target. If the tolerances are not met, resampling of the design space can be carried out or the weights in the optimization problem can be adjusted. When the results have reached the desired accuracy, the next step is to validate the optimal designs using an experimental setup. For the *validation,* an additional tolerance is set which should be higher than the verification tolerance because there is a probability of error propagation through the subsequent steps. If the design reaches the criteria, a design with the desired performance is obtained and the design procedure is successful. Verification, validation, and the case studies are further discussed in Section 3.6.

3. DEM-based metamodel design optimization for a discharging hopper

The metamodel-based design optimization (MBDO) method described in Section 2 is applied to a hopper case study that will be described in this section in more detail. Specific choices made for the various steps are also detailed here. Hoppers are pieces of bulk handling equipment that are frequently used in processing plants to regulate flows of material. In the design of a hopper there are many restrictions such as occupied space and which construction materials can be used in combination with the bulk being processed. However, the key performance indicator (KPI) that is most frequently used to assess the effectiveness of a hopper is the discharge rate.

3.1. Experimental setup and DEM model of hopper

In this study, an experimental setup of a semi two-dimensional hopper is considered which has been shown in Fig. 2. This setup consists of four adjustable stainless steel wall sections which can be used to change the geometry of the hopper. These four adjustable walls are clamped between two 5 mm Perspex plates. The setup is positioned on load cells such that the force exerted by the bulk can be measured. For further information on the experimental setup the reader is referred to Fransen et al., [7]. The load cell data from the experiments is used to determine the discharge rate. In addition, the setup is used to validate the results from the deterministic and robust MBDO. Gravel is used as a bulk material in this experimental setup and was modelled in DEM using spherical particles. The gravel has been stored in a dry environment with a low humidity, therefore we assume the material can be regarded as dry and has no cohesion. In addition, the material falls under the well-graded gravel category for which it is common to take zero cohesion into account (Swiss Standard SN 670010b, Characteristic Coefficients of

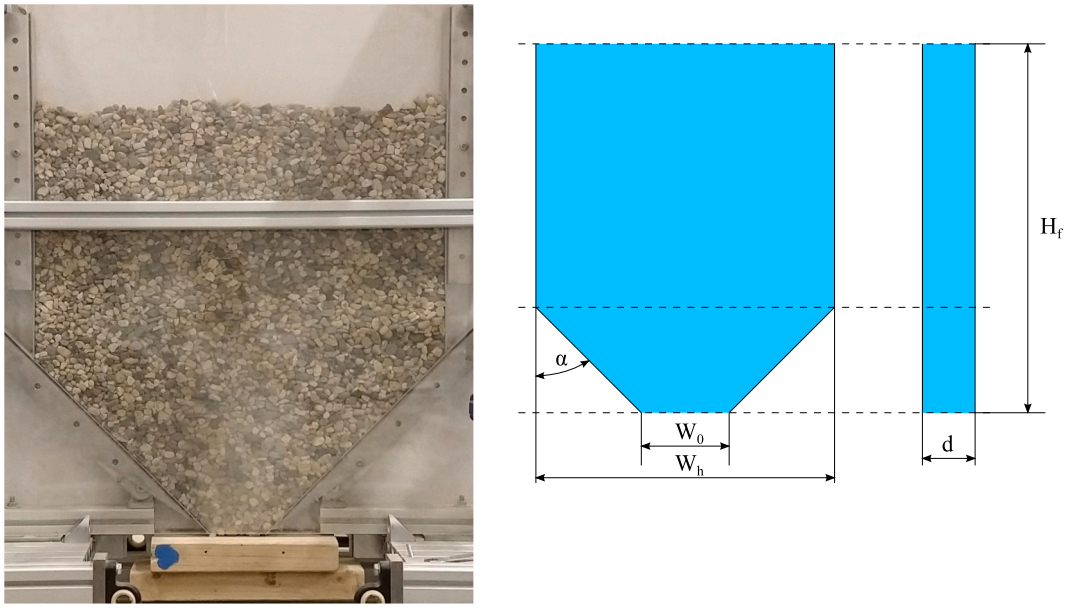

Fig. 2. Experimental hopper setup (a) and dimensions (b) $W_h = 602mm$, $d = 5mm$. The fill height depends on the mass inserted.

soils, Association of Swiss Road and Traffic Engineers). After calibration of the DEM model, the hopper discharge was validated for a hopper configuration with a hopper angle α of 45° and a discharge opening W_o of 100*mm*. The model from this study showed an overestimation for the mean of 2,15% and 42% higher standard deviation. Even though the error in standard deviation is large it is only 1% of the mean. We assume that this level of error is in the same range in the selected design space. The DEM model is used to replicate the experimental setup and to generate a DEM data set for the metamodel. In Fig. 2 (a) an image of the experimental setup of the hopper is shown and a description of the geometry in Fig. 2 (b). In Fig. 3 (a) a still from the initial configuration of an experiment captured with thehigh speed camera is shown and the DEM simulation is shown in Fig. 3 (b).

3.2. Analysis of experimental and DEM simulation results

The KPI of the case study is the steady-state discharge rate ϕ for which both the mean and standard deviation are used. From the hopper discharge experiment the force ($F_{loadcell}$) exerted by the bulk material on the load cell over time is obtained which can be used to determine the steady-state discharge rate. In Fig. 4 (a,b) the process of determining the discharge rate is illustrated for the experimental and DEM data respectively. A difference between the experimental and DEM data is the presence of spikes in the force data. This is explained by the difference in measurement location. The force measurement in the experiment is not located on the walls as is the case for the simulation result but under the base of the setup. The structure between the walls and the load cells has a dampening effect on the forces on the wall and therefore the measurement.

To obtain the average discharge rate in kg/s the average force exerted per second needs to be determined. Assuming this value is stable we can divide this force by the gravity constant (g) to obtain the average mass discharged per second. This value approximates the discharged mass that cannot be measured exactly in the experiment. Even though it is possible to determine the exact mass discharged in a DEM simulation we use the force-based approach because this gives results for experiments and simulations that can be compared. The fitted data between the force based and mass based discharge rate in the DEM simulation showed small deviations and are therefore representative for the performance.

3.3. Sampling of design space and number of repetitions

The design space in this case study is sampled in an irregular spaced rectangular grid for discharge openings of 50, 75, 100, 150, and 200 mm and angles 20, 30, 45, 60, 75, 82.5, and 90 degrees as shown in Fig. 5. For the hopper angles, a minimum of 20 degrees was chosen because of the limits of the experimental setup. At the high end of the angles, an additional sample was added at 82.5 degrees to have a higher information density in this location. The used sample consists of 35 points which means that this sample has a sampling density of $35^{\frac{1}{2}} = 5,92$ per unit length in the normalized design space. This is approximately in the same range as the sampling density used in previous work for a three-dimensional calibration case [7]. For each design point in the sampling we carry out five repetitions to get an average and a standard deviation. This number is enough considering that the discharge rate is already a steady-state value averaged from time dependent discharge data. The results of these simulations are discussed in Section 4.1.

The sample shown in Fig. 5 has also been carried out using the experimental setup. To be consistent with the experiments the number of repetitions is kept the same as with the experiments. At a 150 mm discharge opening and 75 degree angle the number of repetitions is equal to four because of a failed experiment. The same holds for one of 20-degree angle and 75 mm discharge opening experiment. For the 50 mm experiments it was decided to use five repetitions as a basis and extend to ten if arching occurred. In the 60-degree case, arching occurred five times and therefore the additional 5 repetitions were not conducted. The 20-degree case was repeated 10 times but two of those experiments failed. To be consistent with the experiments that have been carried out we used the same initial mass of bulk material contained in the experiment in the simulations and used the same number of repetitions for each design in the sample. In calculating the mean, standard deviation, and confidence intervals the different number of repetitions accounted for.

3.4. Metamodel training

The generated DEM data for the sample of the design space is used to train a Gaussian Process Regression (GPR) type stochastic metamodel [13]. Before the data is used, feature scaling based normalization is used which shifts the data to a [−1,1] range. The standard deviation corresponding to the mean values is converted to the coefficient of variation $\frac{\sigma}{\mu}$ which is input for the σ_n component in the training procedure.

The metamodel is denoted by $G_{KPI}(\boldsymbol{x}^*)$ for any given KPI where $\boldsymbol{x}^*$ is a vector containing the design variables for which a prediction of the mean and variance of the KPI is desired. In the case study, the KPI is the discharge rate and the design variables are the hopper angle α and the size of the discharge opening W_o, $\boldsymbol{x}^* = [\alpha^* \ W_o^*]$. The metamodel is trained with the DEM data generated for the sample presented in Section 3.3 which consist of a mean and variance value of the KPI at the data points in the sample. By including both mean and variance in training the metamodel we allow the metamodel to predict the mean and

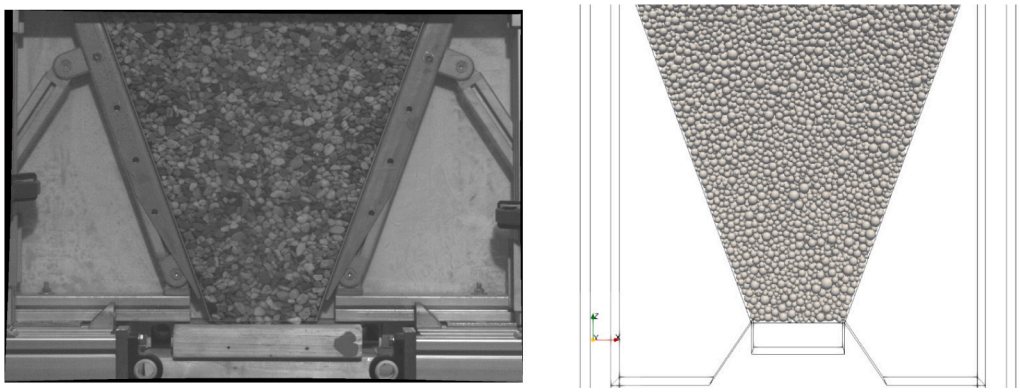

(a) (b)

Fig. 3. (a) Picture of experiment where the block at the bottom prevents the discharge of material (b) Picture of simulation where only the walls and bottom of the experimental setup are modelled.

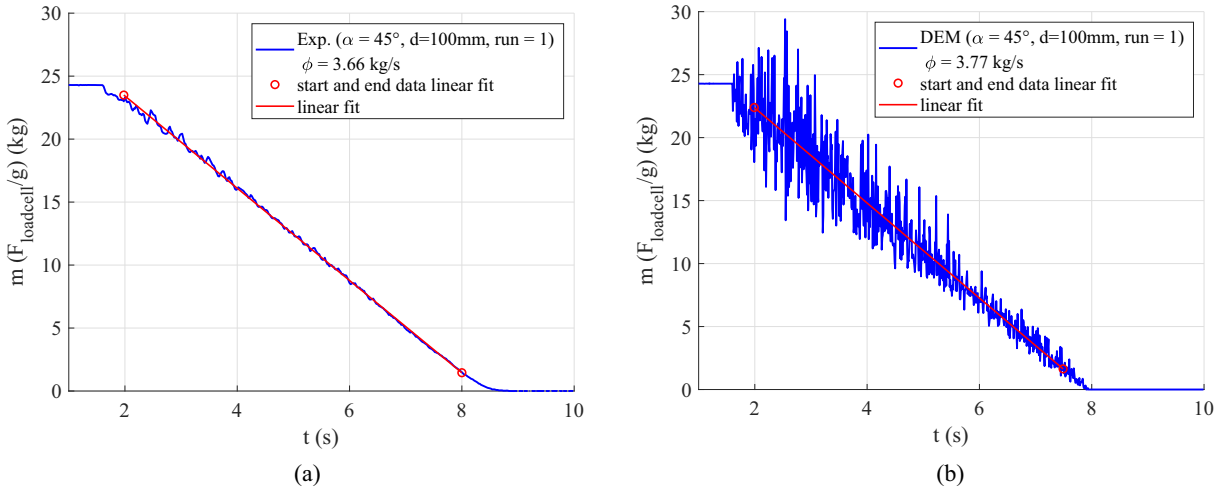

Fig. 4. Determining discharge rate from load cell data (a) and from the simulation of the same experiment (b).

variance. In training the metamodel we assume that the variance obtained in the data points from the training set is the true variance [7]. Thus, the trained DEM-based metamodel gives a prediction of the mean and the variance in the design space.

The GPR metamodel uses a basis function to obtain the correlation between two points $\boldsymbol{x}_1$ and $\boldsymbol{x}_2$. Here $\boldsymbol{x}_1$ and $\boldsymbol{x}_2$ can both be training points, two prediction points, or a training and a prediction point. In this case the basis function is a squared exponential Gaussian ψ in $\mathbb{R}^2$,

$$\psi = \sigma_f e^{-\frac{1}{2l^2} r(\boldsymbol{x}_1,\boldsymbol{x}_2)^2} \tag{1}$$

where σ_f and l^2 represent the first two hyper parameters and $r(\boldsymbol{x}_1,\boldsymbol{x}_2)$,

$$r(\boldsymbol{x}_1 = [\alpha_1\ W_{o,1}]\ ,\boldsymbol{x}_2 = [\alpha_2\ W_{o,2}]\ ) = \sqrt{c_1(\alpha_1-\alpha_2)^2 + c_2\left(W_{o,1}-W_{o,2}\right)^2} \tag{2}$$

is a function which determines the Euclidian distance between two points, $\boldsymbol{x}_1$ and $\boldsymbol{x}_2$. This distance is determined based on the two design variable values in the two points which are adjusted by the second two hyperparameter values c_1 and c_2. Here c_1 and c_2 function as a shape parameter for the basis function on the design variables α and W_o.

The metamodel $G_{KPI}(\boldsymbol{x}^*)$ is used for mean and variance prediction of the KPI. The mean prediction function,

$$G_{KPI}\ (\boldsymbol{x}^*) = k_{KPI}(\boldsymbol{x},\boldsymbol{x}^*)^T\left(K_{KPI}(\boldsymbol{x},\boldsymbol{x}) + \sigma^2_{KPI,n} I\right)^{-1} \boldsymbol{y}_{KPI} = \begin{bmatrix} \psi(\boldsymbol{x}_1,\boldsymbol{x}^*) \\ \vdots \\ \psi(\boldsymbol{x}_n,\boldsymbol{x}^*) \end{bmatrix}^T \left(\begin{bmatrix} \psi(\boldsymbol{x}_1,\boldsymbol{x}_1) & \cdots & \psi(\boldsymbol{x}_1,\boldsymbol{x}_n) \\ \vdots & \ddots & \vdots \\ \psi(\boldsymbol{x}_n,\boldsymbol{x}_1) & \cdots & \psi(\boldsymbol{x}_n,\boldsymbol{x}_n) \end{bmatrix} + \begin{bmatrix} \sigma^2_{KPI,1} & 0 & 0 \\ 0 & \ddots & 0 \\ 0 & 0 & \sigma^2_{KPI,n} \end{bmatrix} \right)^{-1} \begin{bmatrix} y_1 \\ \vdots \\ y_n \end{bmatrix} \tag{3}$$

consists of the correlation between the training points $\boldsymbol{x}_1$ to $\boldsymbol{x}_n$ and the predicted point $\boldsymbol{x}^*$, $k_{KPI}(\boldsymbol{x},\boldsymbol{x}^*)$. Based on the summation of the Gram matrix $K_{KPI}(\boldsymbol{x},\boldsymbol{x})$ and the variances $\sigma^2_{KPI,\,n}$ of the system and the reference values $\boldsymbol{y}_{KPI}$ in the training points a prediction is made for the mean value. The variance predictor,

$$\begin{aligned} V_{KPI}(\boldsymbol{x}^*) &= k_{KPI}(\boldsymbol{x}^*,\boldsymbol{x}^*) - k_{KPI}(\boldsymbol{x},\boldsymbol{x}^*)^T\left(K_{KPI}(\boldsymbol{x},\boldsymbol{x}) + \sigma^2_{KPI,n} I\right)^{-1} k_{KPI}(\boldsymbol{x},\boldsymbol{x}^*)^T \\ &= k_{KPI}(\boldsymbol{x}^*,\boldsymbol{x}^*) - \begin{bmatrix} \psi(\boldsymbol{x}_1,\boldsymbol{x}^*) \\ \vdots \\ \psi(\boldsymbol{x}_n,\boldsymbol{x}^*) \end{bmatrix}^T \left(\begin{bmatrix} \psi(\boldsymbol{x}_1,\boldsymbol{x}_1) & \cdots & \psi(\boldsymbol{x}_1,\boldsymbol{x}_n) \\ \vdots & \ddots & \vdots \\ \psi(\boldsymbol{x}_n,\boldsymbol{x}_1) & \cdots & \psi(\boldsymbol{x}_n,\boldsymbol{x}_n) \end{bmatrix} + \begin{bmatrix} \sigma^2_{KPI,1} & 0 & 0 \\ 0 & \ddots & 0 \\ 0 & 0 & \sigma^2_{KPI,n} \end{bmatrix} \right)^{-1} \begin{bmatrix} \psi(\boldsymbol{x}_1,\boldsymbol{x}^*) \\ \vdots \\ \psi(\boldsymbol{x}_n,\boldsymbol{x}^*) \end{bmatrix} \end{aligned} \tag{4}$$

is a correction based on the prior covariance of the predicted point $k_{KPI}(\boldsymbol{x}^*,\boldsymbol{x}^*)$ minus the information the training points give about the function [13].

As shown in Eqs. (1) and (2), the metamodel has tunable parameters that can be used to improve the quality of the model. The parameters σ_f, l^2, c_1, and c_2 are the hyper-parameters of the basis function and need to be optimized for a good fit of the metamodel to the training data. The σ_f parameter balances the effect of the added noise and l^2 controls the shape of the function. However, the l^2 term is kept constant because the hyper-parameters c_1 and c_2 in the basis function have the same function of controlling the shape of the basis function. Therefore optimizing these three would lead to an undetermined problem. To optimize the hyper-parameters the marginal log-likelihood function,

$$logp\ (y_i|X) = -0.5 y_i^T\left(K_{KPI} + \sigma^2_{KPI,n} I\right)^{-1} y_i - \frac{1}{2} log|K_{KPI} + \sigma^2_{KPI,n} I| - \frac{N}{2} log(2\pi) \tag{5}$$

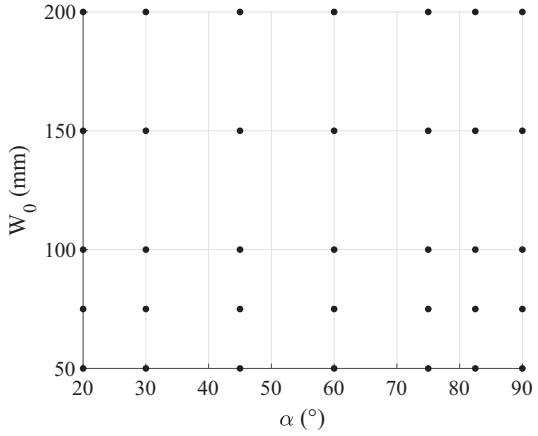

Fig. 5. Sampling grid with five discharge opening sizes and seven hopper angles.

of the metamodel is maximized. Here 100 random initial guesses in a range from 0 to 100 are used to find the optimal set of hyper-parameter values because the log-likelihood function is expected to be nonconvex. To find this set the interior point method is used [1]. The resulting metamodels are discussed in Section 4.2.

3.5. Formulation optimization problem

In essence, the optimization problem for the design of the hopper is similar to the calibration problems described in previous studies [5]. Therefore, most solving methods used in these studies can also be applied in the optimization of design. However, there are distinct differences in the type of solutions that are obtained. When genetic algorithms or other types of swarm methods are used, the design domain is populated with samples which generally evolve over time to a set of solutions. These solutions can form a Pareto-front on which a designer can pick a design which gives the best-balanced solution. A different approach is to let the optimizer find single or several local optimal designs and converge to a set limit as used by Fransen et al. [7] with the interior-point method. This is the method that is used in solving this optimization problem. This optimization is repeated with 100 random initial guesses spread around the design space using Latin Hypercube Sampling (LHS). Using a 100 random initial points ensures that the majority of the local optima is found.

To define the optimization problem we define objective function f for the described optimization problem. This objective function is formulated using the weighted-sum method [12] which is used in robust optimization because of its ease and simplicity. In this case study the multi-objective problem consists of two objectives. The first part of the objective function describes the discharge rate constraint which needs to reach a specified value. The second part of the objective function is the variance objective. The relative importance of these two parts is controlled by the factor β. The solution will focus more on an exact match to the mean if β moves to one whereas a higher focus on the variance is achieved with a small β. This formulation has been chosen because it shows a clear relation between the importance of the mean and its variance. The objective function,

$$f = \beta\left[\frac{\mu_1}{\mu_1^*}\right]^2 + (1-\beta)\left[\frac{\sigma_1}{\sigma_1^*}\right]^2 \tag{6}$$

consists of two components, a mean and standard deviation objective for each KPI. The first component,

$$\left[\frac{\mu_1}{\mu_1^*}\right]^2 = \left(\frac{\phi(\boldsymbol{x}) - \phi_t}{\phi_t}\right)^2 \tag{7}$$

is the square of the relative error between the mean prediction of the discharge rate by the metamodel and the discharge rate target $\phi(\boldsymbol{x}) - \phi_t$ which is divided by the discharge rate target ϕ_t. The second component,

$$\left[\frac{\sigma_1}{\sigma_1^*}\right]^2 = \left(\frac{\sigma(\phi(\boldsymbol{x}))}{max(\sigma(\phi(\boldsymbol{x})))}\right)^2 \tag{8}$$

is the square of the ratio between the predicted standard deviation of the discharge rate and the maximum standard deviation of the discharge rate present in the model. This ensures that the standard deviation is minimized in a range from zero to one.

3.6. Case studies including verification and validation

In this paper we will look at two case studies which are representative of a hopper design case. The optimization problem described in the previous section will be solved for these two cases. For both cases we will use a threshold in the verification error of 5% and for the validation the results should remain within a 10% threshold to cover error propagation between the verification and validation step. These cases will be a discharge rate target of 4 kg/s (Case 1) and 8 kg/s (Case 2). For the deterministic optimization, the coefficient β is equal to one and for the robust optimization case the coefficient $\beta = \frac{5}{6}$ which corresponds to a 5:1 ratio between the mean and variance. This ratio has been chosen because the actual discharge rate of the hopper is the essential performance indicator. The variance is an additional measure that focusses the optimization into the direction of a reliable design and therefor has a smaller coefficient. Using a ratio of 1:1 would likely result in a design optimum with a large mismatch to the targeted discharge rate. The two discharge rate cases are used to show difference between deterministic and robust optimization by only considering the discharge rate KPI. These results will be discussed in Section 4.2.

To put the case studies into context with an industrial setting we have to address the following. Relative to industrial scale hoppers, the size of the hopper used in this case study is small. However, results from this study serve as a proof of concept and might lead to opportunities for research focussed on scaling and validation on a pilot-scale, and later on to the industrial scale. In addition, more complex bulk materials including cohesion and other inter-particle behaviour are interesting topics.

4. Results

In this chapter the results from the metamodel training and optimization studies described in Section 3 are presented. First we analyse the DEM simulation data and evaluate the trained DEM-based metamodel. Next, the results of deterministic and robust design optimization approaches for the discharge rate and its standard deviation as the objectives are discussed. This section also includes the verification and validation of the optimization results.

4.1. DEM data and DEM-based metamodel

The training data for the DEM-based metamodel consists of DEM data for the discharge of a hopper. In Fig. 6(a) the discharge rates obtained from the DEM data set used for metamodel training is shown combined with a surface plot of the trained metamodel. For the discharge rate in Fig. 6 (a) we can observe an approximately linear relation between the hopper angle and the size of the discharge opening but with different gradients. Fig. 6 (b) depicts the standard deviation of the average discharge rate from the simulations and the predictions by the metamodel. This clearly shows that the standard deviation is high for the 50 mm discharge openings. This is most likely related to the slow and irregular discharge process and the possibility of arch formation as is discussed in more detail in Appendix A.1. For the 75 and 100 mm

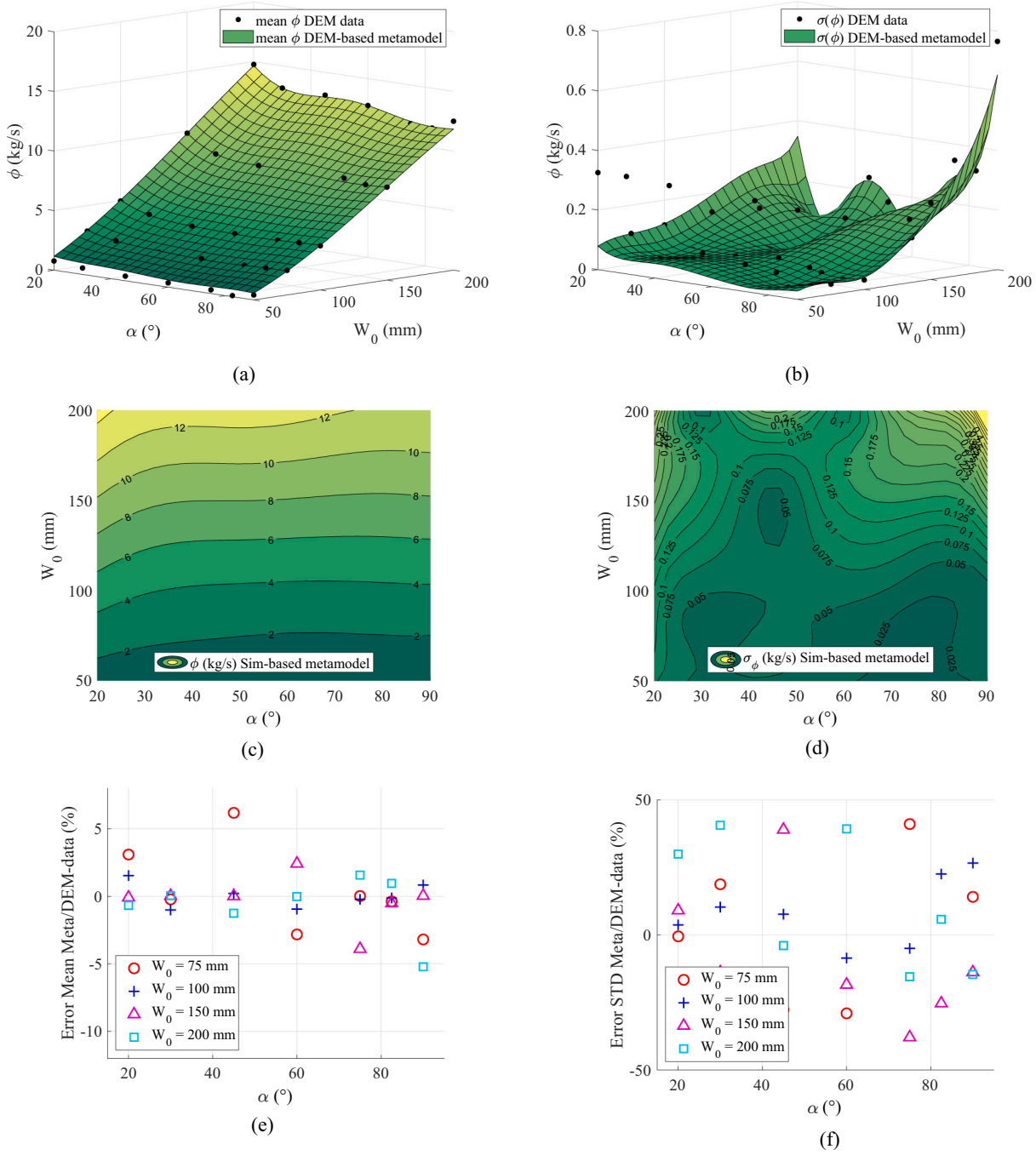

Fig. 6. Surface plots of the mean and standard deviation predictions by the metamodel (a,b) contour plots of the mean and standard deviation (c,d) and the percentage error between the DEM-based metamodel predictions and DEM data for mean and standard deviation (e,f).

Table 1
Coefficients of Gaussian Process Regression Metamodel

Metamodel	σ_f	l^2	c_1 (α dir.)	c_2 (W_0 dir.)
G_{DR} Discharge rate	1.797	1	1.201	0.166

discharge openings we see similar levels of variation, up to 0,1 kg/s, which starts to increase again with increasing discharge openings. At the 60- and 75-degree hopper angles we see low variation in the discharge rate for the higher discharge openings.

Based on the mean and standard deviation of the discharge rate the Gaussian Process Regression (GPR) metamodel is trained as described in Section 3.1. This leads to the coefficients for the GPR for the discharge rate listed in Table 1. Together with the provided dataset, these values allow the GPR metamodel, G_{DR}, to be reconstructed. Based on the large difference between c_1 and c_2 the included flexibility for different parameters is justified.

In Fig. 6 (c,d) the contour plots of the mean and standard deviation predictions by the DEM-based metamodel are shown. Fig. 6 Fig. 1 (c) shows isolines of constant discharge rate and exhibiting a near linear relation with the discharge openings based on the distance between the isolines as was also visible in the DEM data. The dependency on the hopper angle shows a slightly curved relation. Fig. 6 (d) shows the standard deviation where regions of low standard deviations are visible indicating areas containing reliable designs.

Visually it is difficult to assess the errors made in predicting mean and standard deviation of the discharge rate in the design space. Therefore the percentage error in prediction is depicted in Fig. 6 (e,f) for the mean and standard deviation respectively. Here the error percentages for the 50 mm discharge opening are left out because these percentages are very high for both mean and standard deviation. This can be explained because all simulations at the 50 mm discharge opening encountered arching at one point during the simulation leading to high errors. This is highly undesirable in a hopper design and therefore it is not likely that design solutions for the prescribed cases will be found in this region. In the remainder of the design space, the variance prediction is reasonably accurate and follows the trend in the data and therefore deemed good enough to be included in the optimization. For further information on the arching phenomena in the simulations we refer to Appendix A.1. In Fig. 6 (e) it is seen that the error for the 75 mm discharge opening varies greatly with the hopper angles. An over or under estimation of at most 6% of the discharge rate is expected for most angles except for the 30, 75, and 82.5 degree angles. As is the case with the 50 mm opening, the 75 mm opening DEM simulations encountered arching as well but not for all simulations. For the 100 mm discharge opening we see that the fit is accurate within 1.5%. At 150 mm the metamodel is accurate except for the 60 and 75-degree hopper angles which look at errors of at most 6%. For the 200 mm discharge opening the error is within 1.5% except for the 90-degree angle.

In Fig. 6 (f) the error in standard deviation prediction shows significantly higher values than for the mean prediction. This was already clearly visible in Fig. 6 (a) where large differences between the training data and the metamodel surface were seen. As a results the error fluctuates quite severely between −40 and +40% throughout the design space. Even with these high fluctuations, Fig. 6 (a) shows that the metamodel is able to follow the trend in the data which is essential for robust optimization. However, for the application it is important that the prediction of the standard deviation is also accurate. Even though it can be used, the analysis of the metamodel and DEM-data clearly indicates that for quantitative prediction, the reliability of the standard deviation should be increased by increasing the number of repetitions of the DEM simulations in each data point.

Overall, in most regions of the design space the mean prediction error is well below 3% with some exceptions reaching 6%. Based on these errors in mean prediction and the trend presented by the metamodel for the standard deviation, we proceed with using the metamodel in deterministic and robust optimization.

4.2. Deterministic vs robust design optimization

To identify the effect of using deterministic and robust design optimization (DO) two case studies are investigated. In these case studies we optimized a hopper design using deterministic and robust optimization for a discharge rate of 4 kg/s (Case 1) and 8 kg/s (Case 2). In Fig. 7 the contours of the discharge rate (a) and standard deviation (b) are visualized in the design space. The magenta and red coloured dots are the results from the deterministic optimization for Case 1 and 2. The yellow and blue dots represent the solutions for the robust optimization for Case 1 and 2.

The deterministic optimization results clearly show that solutions are not unique and present a wide variety of design options with the same performance. Based on the single objective for the discharge rate in both cases the solver will return solutions on the isoline for the corresponding discharge rate, which represents designs of equal performance. However, the solutions for both cases are all located in the middle of the isolines and not at the outer hopper angles even though the solutions would give the same result. This can be explained by the interior point method which uses a barrier function that initially promotes searching the interior of the domain.

The robust optimization results for cases 1 and 2 including the variance as a second objective clearly show more distinct solutions compared to the deterministic results. The robust optimization results for case 1 show three distinct optima of which the 81 degree and 104 mm design has the lowest variance followed by the 44-degree and 103 mm and 31-degree and 98 mm design. The location of the robust designs in Fig. 7 (b) shows a clear minimum in variance for the 45-degree solution in Case 2 and shows that the other solutions are located at points where there is large curvature in the isoline of the standard deviation. The exact designs and performance of the robust optima are shown in Table 2. Comparing the two cases shows that there are two solutions with a similar angle in both cases: the 45- and 81-degree hopper angle where only the size of the discharge opening is different. The 31-degree angle present in case 1 is not present in Case 2. Additionally, it is visible that there is a small difference between the target discharge rate compared to the deterministic results. This is caused by the additional objective for which the optimizer has to start making a trade-off. The 81-degree solution for Case 2 shows a discharge rate difference of about 2% and also the largest standard deviation, which indicates this is a poor local minimum.

Comparing the deterministic and robust optimization results, we see that only the 45-degree solutions in the robust optimization are present in the deterministic results. The solution at 31 and around 80 degrees are not present when using the interior-point-method but might become

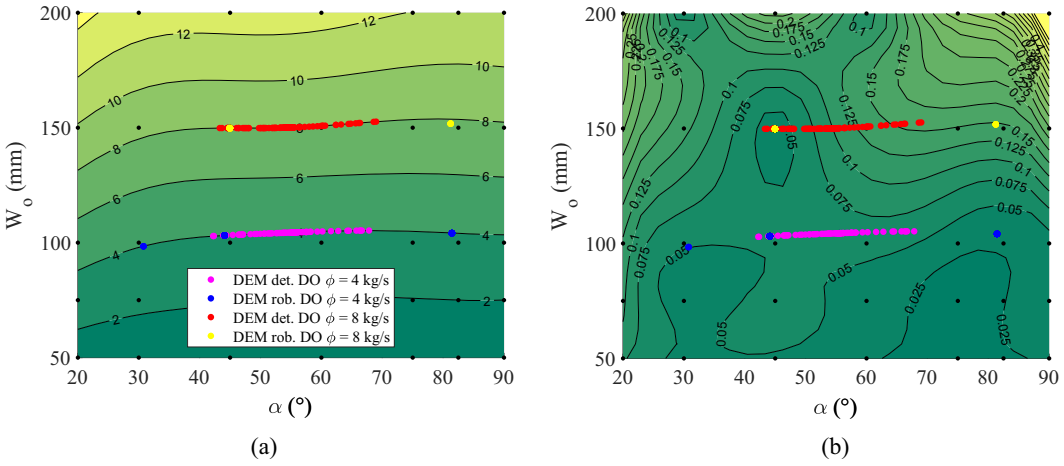

Fig. 7. Deterministic and robust optimization results for both the 4 kg/s and 8 kg/s discharge rate target.

Table 2
Local optima for robust optimization results with the corresponding average and standard deviation of the discharge rate

	Hopper angle α (°)	Discharge opening $W_o(mm)$	Average discharge rate $\phi\left(\frac{kg}{s}\right)$	Standard deviation discharge rate $\sigma(\phi)\left(\frac{kg}{s}\right)$
Case 1: 4 $\left(\frac{kg}{s}\right)$	30.77	98.42	3.994	0.05
	44.11	103.2	3.999	0.051
	81.45	104.1	3.997	0.032
Case 2: 8 $\left(\frac{kg}{s}\right)$	44.96	149.8	7.993	0.039
	81.23	151.8	7.84	0.147

visible when different search algorithms are used. In the deterministic case, the standard deviation information from Fig. 7 (b) is not used but by projecting the solutions it can be seen that using the standard deviation by means of robust optimization could be used to make design decisions from the deterministic optimization results.

Based on the deterministic optimization results a design between 42- and 69-degree hopper angles with their corresponding widths would result in a hopper with the right performance for both Case 1 and 2. For the robust optimization, we would have three hopper designs for Case 1 and two solutions for Case 2. For both Cases there are solutions around a 44- and 81-degree hopper angle that would be suitable where the 44-degree design is equally reliable for Case 1 and 2 but the 81-degree design only for Case 1. However, these designs are only based on the performance of the design and do neglect other aspects which would be encountered in engineering and operation of the equipment. For example, with an 81-degree angle stagnant zones would form on the slopes of the hopper walls because friction with the wall keeps the material in place. This would lead to a core flow dominated hopper which decreases wear of the equipment but might increase material wear. On the contrary, a 44- or 31-degree angle would lead to flow along the walls and a mass flow dominated hopper performance with increased equipment wear for abrasive materials but less material wear. Numerically, it would be clear that the 44/45 degree angle would lead to the most reliable performance for Case 2 but if engineering and operational aspects are considered one of the other designs might be chosen. In Appendix A.2, an elaboration can be found on design considerations in hopper design.

4.2.1. *Verification of deterministic and robust optima*

As part of the method described in Section 2 the results from the deterministic and robust optimization are verified. The metamodel predicted a discharge rate isoline for both cases in the design space of the hopper. This resulted in the deterministic optimization procedure to find a distribution of points on this isoline. Instead of verification of all these points on the isoline we decided to verify the metamodel prediction at 8 points along the isoline distributed from 20 to 90 degrees with a 10-degree interval with their corresponding discharge openings as found in Table 3. For each of these points the DEM simulation is repeated 5 times with an initial random packing of particles.

In Fig. 8 (a) and (b) the mean (blue dots) and 95% confidence interval (CI) of the mean (blue envelope) are shown as predicted on the isoline by the DEM-based metamodel for both cases. In addition, the verification results of the mean and 95% CI of the mean are shown. Overall, it can be seen that the verification results show good resemblance with the predicted results by the DEM-based metamodel for the isolines of 4 and 8 kg/s. Most of the designs on this isoline will be within 2,5% of the prediction which is acceptable looking at the set tolerance of 5%. The 95% CI from the verification results shifts with the location of the mean but overall the behaviour in variance is similar to the predictions by the DEM-based metamodel. Some exceptions in the behaviour are discussed below. Considering the limited number of repetitions, these results are promising for use of DEM-based metamodels in design optimization for bulk handling equipment.

In Case 1 it is clearly visible that at the 90-degree hopper angle the mean has an error of 5% as well as a wide 95% CI. The second simulation for the 20-degree point encountered arching directly at the start of the simulation, therefore it is not included in calculating the discharge rate in this point. For the third simulation the same occurred but when the half of the hopper had already discharged. This was long enough for calculating the discharge rate and is therefore included. However, it must be noted that with the 20-degree case there is a high likelihood of arching so it is not a reliable design point. Another simulation that shows a large error with the predicted discharge rate is the second simulation for the 90-degree angle case. During the discharge of the hopper the mass flow slows down halfway during the discharge but comes up to speed again, leading to a lower average discharge rate. This slight plateau forming also occurred with the second and third simulation for the 30-degree angle. The likelihood of arching increases with decreasing discharge opening sizes which is clearly the case for the 20-degree hopper angle. Plateau forming or stalling during discharge is a phenomenon that can ultimately lead to arching so it is not strange that this occurs at the 30-degree angle and is likely to become more severe with a decreasing discharge opening size. In the 8 kg/s case we do not observe arching which can be explained by the fact that the discharge openings never reach the sizes in which arching starts to occur. This case shows that at 20-, 50- and 60-degree angles the verification results are matching the DEM-metamodel prediction. For the 40-, and 70- to 90-degree angles we see an overestimation of approximately 2.5% for the mean discharge rate. One exemption is the 30-degree angle, which shows a 5% overestimation. The confidence interval shows approximately the same behaviour as predicted but is on average wider than predicted.

In addition to the verification of the deterministic results the robust optima are also verified. Therefore 5 repetitions of the DEM model simulation for each local optimal design have been carried out as was the case for the generation of the DEM data for the metamodel. The error percentages for the verification of the robust optima are shown in Table 4. For visualization, these results are combined with the deterministic results in Fig. 8 where in (a) the verification results for Case 1 are shown and (b) shows Case 2. The green dot represents the predicted mean for each optimum and the green rectangle represents the 95% CI of the mean in this location. The Case 1 discharge rate verification results show that the mean for the 31 degree hopper angle is a closely matches the predicted optimal mean. However, the 95% CI is 1.7 times wider than for the predicted mean. For the other two optima it can be observed that the metamodel predicts a higher mean than the verification results.

Table 3
Verification design points along the 4 and 8 kg/s discharge rate isoline predicted by the metamodel

α(°)	20	30	40	50	60	70	80	90
Case 1 W_o (mm)	87.9	97.9	102.4	103.9	104.9	105.2	104.4	103.4
Case 2 $W_o(mm)$	131.5	145.1	149.6	149.8	150.8	152.8	153.7	152.4

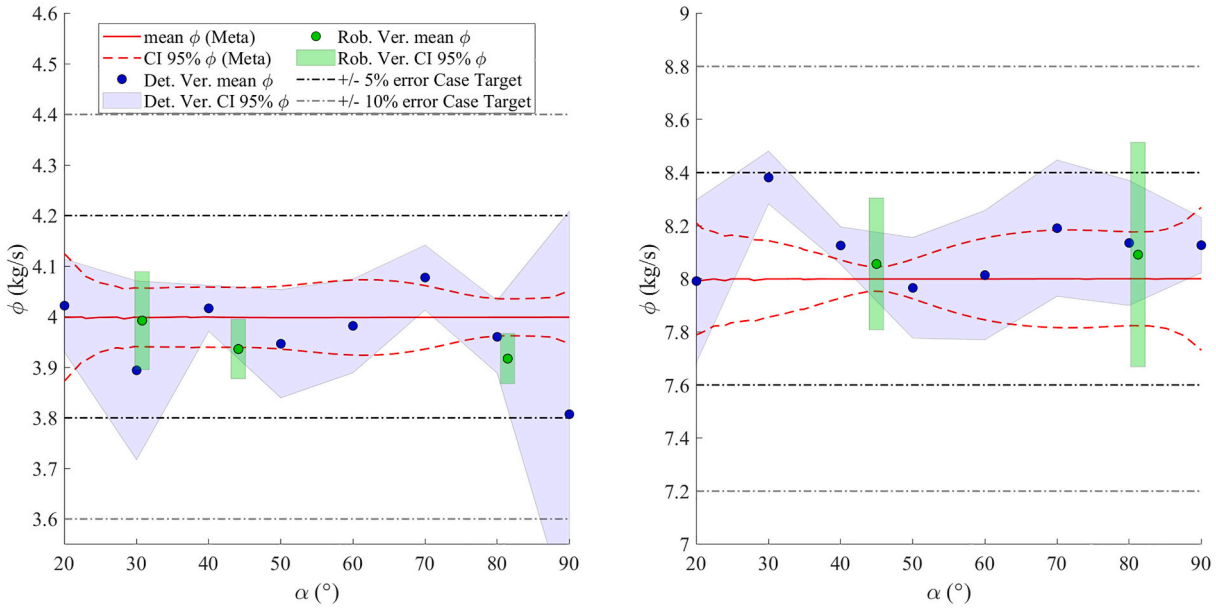

Fig. 8. Verification results of isoline verification points for 4 kg/s (a) and 8 kg/s discharge rate (b).

Table 4
Local optima for verification of the robust optimization results with the corresponding average and standard deviation of the discharge rate

	Average discharge rate $\phi\left(\frac{kg}{s}\right)$	Standard deviation discharge rate $\sigma(\phi)\left(\frac{kg}{s}\right)$	% error with mean robust optima	% error with standard deviation in robust optima
Case 1:	3.992	0.084	-0.044	70
4 $\left(\frac{kg}{s}\right)$	3.936	0.051	-1.575	4
	3.917	0.043	-1.999	35
Case 2: 8 $\left(\frac{kg}{s}\right)$	8.056	0.216	0.786	453
	8.091	0.368	3.199	150

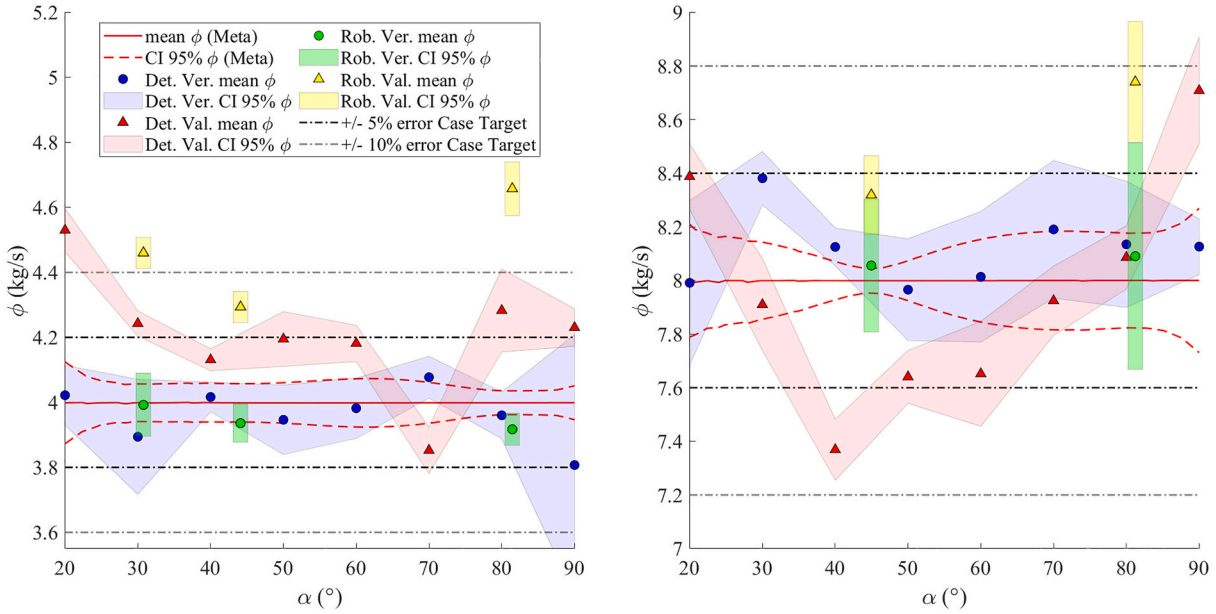

Fig. 9. Mean and 95% CI predicted by DEM-based metamodel, verification and validation from the deterministic and robust optimization with 5 and 10% error margins with respect to the mean target for Case 1 and 2 in (a) and (b) respectively.

The difference between prediction and verification is 1.6% and 2% for the 45- and 81-degree case, respectively. The CI of the 44-degree case is the same in magnitude but shifted due to the error in the mean. For the 81-degree case the CI is 35% wider than predicted and shifted due to the large error in the mean.

For Case 2 we see that at the 45-degree hopper angle the verified mean is 0,8% higher than predicted. In the 81-degree case this is 3,2% but here it should be observed that the found optima was already slightly off from the target and that the verification results are closer to the initial optimization target. In terms of the CI it can be seen that it is wider in both cases up to 4.5 times for the 45-degree angle. Considering the mean prediction we would accept these optima because they are within the 5% tolerance that we have set even though the confidence intervals show significant errors. However, for a full evaluation it is important to study how the optima of both cases behave when these are experimentally validated.

4.2.2. Validation of deterministic and robust optima

We performed validation of the deterministic and robust optimization results by means of experiments using the setup introduced in Section 3.1. For the validation of the DEM-based metamodel prediction the same designs as for the verification simulations are used. Here it is important to notice that the hopper angle and size of the discharge opening in the points presented in Table 3 cannot be set exactly because of the measurement error of the angle (+/− 0,1 degree) and discharge opening (+/− 1 mm) of the physical setup. In Fig. 9 (a) and (b) the DEM-based metamodel prediction for the discharge rate for Cases 1 and 2 are shown combined with the verification results. These are the same as shown in Fig. 8 but the validation results for the deterministic and robust optimization are added. The validation results for the deterministic optimization are represented by the red triangles for the mean and the red shaded area for its 95% confidence interval. For the robust optimization results yellow triangles are used and the yellow shaded area represents its 95% confidence interval. Fig. 9 In addition to these visual results the percentage errors with the optimization target are presented in Table 5.

Overall we can see that the DEM-based metamodel and the DEM model itself underestimate the actual discharge rate of a design in both the deterministic and robust cases. However, in the preceding verification it was found that the DEM-based metamodel is relatively accurate in predicting the outcome of a DEM simulation for both the mean and its confidence interval. The validation results indicate that the DEM-based metamodel predictions are closer to experimental results in the region of Case 2 of the design space than for Case 1.

For deterministic Case 1 the largest mean error between the DEM-based metamodel prediction and the experimental results is present at a 20-degree angle and is about 13%. In the 30- to 60-degree angle range the error fluctuates between 3.5 and 6.5%. At 70 degrees it is observed that the error in mean prediction is around 4%. Remarkably, this is the only design for which an underestimation of the discharge rate is observed in the validation even though the load cell data is consistent. For the 80- and 90-degree angles we see 6 to 7.5% errors. The robust Case 1 validation results show an error of 12% for the 31,8-degree hopper angle, 7,5% for the 45-degree angle and 16,5% for the 81-degree angle. All of these results show that the found robust optima underestimate the actual discharge rate. Relative to the deterministic validation results the robust validation result shows an higher error. In terms of the 95% confidence interval it can be seen that this is similar for the predicted 95% CI by the DEM-based metamodel and even slightly smaller.

The validation results of deterministic Case 2 shown in Figure 9 (b) show a maximum error at the 90-degree hopper angle of around 9%. At the 40-degree hopper angle the error in mean prediction is around −8%. All the other errors are within the 5% error margin. In terms of the 95% confidence interval we see that it is twice as small as the predicted width of the confidence intervals by the DEM-based metamodel. For Case 2 the DEM-based metamodel predicts local optima at the 45 and 80-degree hopper angles. The validation results seem to show the same behaviour which reinforces the idea of quantatively using the variance in robust optimization. For the robust optima it can be seen that the 45-degree optimum has an error of around 4% and the 81-degree angle a 9% error. The 95% CI of the first optima is 230% as wide as the prediction by the DEM-based metamodel whereas for the second optimum the error is only 33% wider than predicted. This indicates that predicting confidence intervals is difficult, especially with a low number of repetitions.

In both cases relatively large errors are observed in the validation results whereas the verification results did not show these to the same extent. The source of this difference can be explained by comparing the DEM data to experimental results in the same data points. This shows that the 2% error obtained from the calibrated DEM model at a 45-degree hopper angle and 100 mm discharge opening is not consistent throughout the design space. In Appendix A.3 these results are compared in more detail. These results showed that the error between DEM and experimental data is not consistent throughout the design space. When the DEM model cannot produce accurate predictions in the entire design space, increased errors in the performance of optimized designs can be expected.

Comparing the validation results from both cases it is observed that the validation error of the mean prediction by the DEM-based metamodel stays within the 10% error threshold for Case 2. For Case 1 we see that in most locations the error stays within 10% of the DEM-based metamodel prediction except for the 20-degree hopper angle and the first and third robust optima. In terms of acceptance of the solutions on the isolines we would accept most solutions if the 10% error threshold for the validation was considered. However, the results clearly show that the error at the 20-degree angle is significantly larger than for the other solutions. These results indicate that there is a significant error between the experiment and the DEM-model even though it has a 2% error based on the calibration [7]. Based on the trajectory of the isoline results it is clear that the error is not consistent throughout the design space. This means that the assumption of uniform errors throughout the design space cannot be made. Explanations for this inconsistency are the different flow velocity regimes in the different designs which are not considered in the calibration.

Based on the validation results we can assume that the DEM-based metamodel optimization results for Case 2 can all be used and for Case 1 only in the range from 30 degrees and higher even though the robust optima showed errors higher than 10%. From a deterministic optimization perspective all designs in these regions would be

Table 5
Local optima for validation of the robust optimization results with the corresponding average and standard deviation of the discharge rate.

	Average discharge rate $\phi\left(\frac{kg}{s}\right)$	Standard deviation discharge rate $\sigma(\phi)\left(\frac{kg}{s}\right)$	% error with mean robust optima DEM-based metamodel prediction	% error with standard deviation in robust optima
Case 1:	4.46	0.042	11.67	-16.75
4 $\left(\frac{kg}{s}\right)$	4.29	0.042	7.36	-18.35
	4.66	0.072	16.52	124.11
Case 2: 8	8.32	0.127	4.08	226.45
$\left(\frac{kg}{s}\right)$	8.74	0.196	11.49	33.35

acceptable. For the robust optimization results only the 45-degree design for Case 1 would be acceptable as are both solutions for Case 2. A question that should be asked is whether the optimization is actually robust if errors seep in the method by means of the quality of the data, DEM-model, and metamodel. However, the small errors between DEM-based metamodel predictions and the verification results for a small number of repetitions shows that MBDO using a DEM-based metamodel has potential.

5. Conclusions

In design of bulk handling equipment the stochastic nature of granular material behaviour is rarely included as is the use of metamodel-based design optimization (MBDO). Therefore this study investigates the effect metamodel-based deterministic and robust optimization strategies have on hopper design optimization. Both strategies use DEM-based metamodels for the prediction of mean and variance and are verified and validated by the DEM equipment model and experiments, respectively. The goal of this study is to introduce a robust MBDO, identify the differences between deterministic and robust optimization strategies and the challenges that might be encountered.

The deterministic and robust design optimization case studies show that for deterministic optimization a multitude of local optima are distributed over the isoline of the desired discharge rate whereas the robust optimization zones produces more specific solutions by using the variance. The verification of the deterministic optimization results showed an error in mean prediction within a 5% bandwidth, whereas the errors found in robust optimization results did not exceed 2,5%. The confidence intervals showed more fluctuation and are therefore less reliable. However, based on the mean prediction it seems that robust optimization leads to better performing optima.

One common issue in the use of metamodels in a design process is the effect of error propagation due to a mismatch between the metamodel and the data it is trained on. This is true for metamodels that predict a mean or both mean and variance and is directly affected by the reliability of the used mean and variance training data. In addition, the optimization results are affected by a mismatch between DEM model and experiments. These errors became clearly visible in the verification and validation stage of the deterministic and robust optimization results.

Overall, the use of DEM-based metamodels gives insight on the behaviour of bulk handling equipment which can be used for finding suitable designs in the design space. For bulk handling systems with multiple design and performance parameters and similar problems in other domains, design optimization strategies such as the deterministic and robust approach are good options to find a range of optimal designs. The robust optimization finds designs which in addition to optimized mean performance also exhibit low variance. However, the quality of the optimization relies highly on the quality of the mean and variance data that is available for the metamodel. This is one of the biggest challenges in applying robust MBDO in design of bulk handling equipment.

CRediT authorship contribution statement

Marc P. Fransen: Conceptualization, Methodology, Software, Validation, Formal analysis, Investigation, Writing – original draft, Project administration, Visualization. **Matthijs Langelaar:** Supervision, Writing – review & editing. **Dingena L. Schott:** Supervision, Writing – review & editing.

Declaration of Competing Interest

The authors declare that they have no known competing financial interests or personal relationships that could have appeared to influence the work reported in this paper.

Data availability

Data will be made available on request.

Appendix A. Appendix

In the article we focussed on the differences between MBDO in case of deterministic and robust optimization. However, in designing bulk handling equipment specific phenomena occur such as arching which is possible in all equipment where narrowing channels for granular flow are used. In Appendix A.1 the occurrence and causes of arching in both simulations and experiments are evaluated. Next, Appendix A.2 discusses the design considerations one can make in deciding which design is optimal for a specific application. Lastly, Appendix A.3 discusses the mismatch between the DEM-data and the experimental data which was also apparent in the presented verification and validation results.

A.1. Arching

As mentioned at the beginning of this section arching may occur at small discharge openings if the discharge opening is smaller than ten times the average particle diameter [18]. For the case study this means that the minimum size of the discharge opening should be 100,4 mm. However, in the design space also 50 a 75 mm size samples are included. In Fig. 10 the occurrence of arching in both experiments and simulations is shown for each hopper angle for the 50 mm discharge opening in (a) and 75 mm discharge opening in (b). In the experiments it was observed that at a 60-degree angle and 50 mm discharge opening arching occurs at each instance. For an increasing and decreasing angle we see that the probability of forming of arches reduces. In contrast, in the DEM simulations arches form for each simulation at 50 mm discharge openings. Looking at the 75 mm discharge opening results it can be seen that the simulations show arching at small and large angles but no arching at a 75-degree angle. This behaviour is exactly opposite to the experimental results with a 50 mm discharge opening. These results indicate that the DEM model is not able to reproduce a phenomenon such as arching accurately. Moreover, these results show that validation of calibration results is important and that multiple KPIs should be verified and

validated.

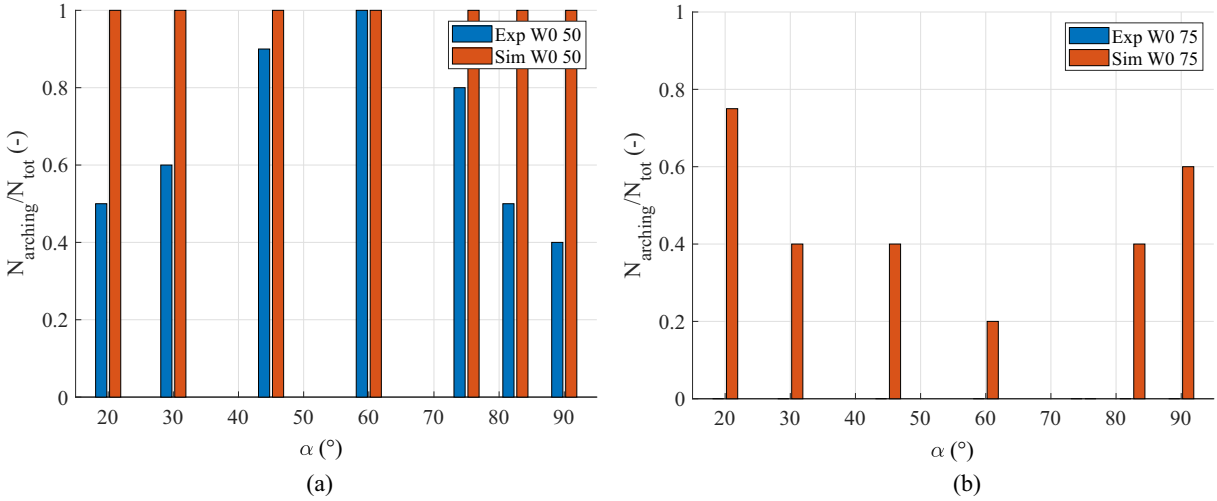

Fig. 10. Arching in the hopper for experiments and simulations for 50 mm discharge opening (a) and 75 mm discharge opening (b).

A.2. Design considerations

In design optimization of bulk handling equipment it is important to consider additional behaviour of material and equipment in assessing the found optima. One of these phenomena was arching which was described in A.1. In bulk handling equipment the interaction between material and structure is not only determined by the geometry but also by the condition of the structure. The stainless steel wall in the hopper geometry is impact loaded and has a friction coefficient of 0,52 which results in a friction angle of 27,5-degrees. In Fig. 7 showing the contour plots, this means that all points around the 62,5-degree angle are likely to show stick slip behaviour. For angles below 62,5-degrees there is continuous movement of particles and possibility of mass flow. Whereas, above 62,5-degrees, stable stagnation zones and core flow will occur. In Fig. 7 showing the optimization results for Case 1 we see that the 30 and 45-degree solutions for the DEM data will likely be mass flow. However, the third solution for the DEM data is at an 80-degree angle which is likely in the core flow regime. With respect to the design choice in the DEM solution of Case 1 the choice is not limited to the discharge rate and its variance but also to the type of system that is desired. If the material that is put through the hopper has an abrasive nature, the mass flow designs are not convenient because they would increase equipment wear. This means that the core flow design would be the correct choice. However, it can be argued that friction between particles is not desired because of material wear making the mass flow designs the better option despite the lower variance in the core flow design. It is important that when the design is chosen the optimization result is not blindly accepted because other aspects of the design in operation should be considered.

A.3. Comparing DEM results and experiments

The validation results in this study showed differences in predicted discharge rates between the DEM-model simulation results and experiments. Based on the calibrated DEM-model an overestimation of 2% was expected by the DEM-model compared to the experiments. However, this error seemed to be inconsistent throughout the design space as shown by the validation results. In Fig. 11 (a,b) we have shown the average discharge rate and its standard deviation based on the DEM-data and their equivalent experiments using five repetitions for the sampled design space along with the respective errors for each discharge opening and angle in Fig. 11 (c). As can be seen the results from the calibration is a 2% error at a 45-degree angle and 100 mm discharge opening. As can be seen for the other angles for the 100 mm discharge-opening errors up to 6% are present. This means that if the DEM model is used to predict the discharge rate for a 20-degree angle and 100 mm discharge opening the result is 5% higher than the value obtained from the experiments. However, getting closer to the 75 mm discharge opening leads to an underestimation of 5%. This means that significantly larger errors between DEM-model and experiment are present in different parts of the design space than expected from the calibration [7]. Combined with the introduced error by the DEM-based metamodel this can lead to additional errors in the different steps in the methodology. To prevent this, additional calibration experiments can be used to resemble the physics of the system.

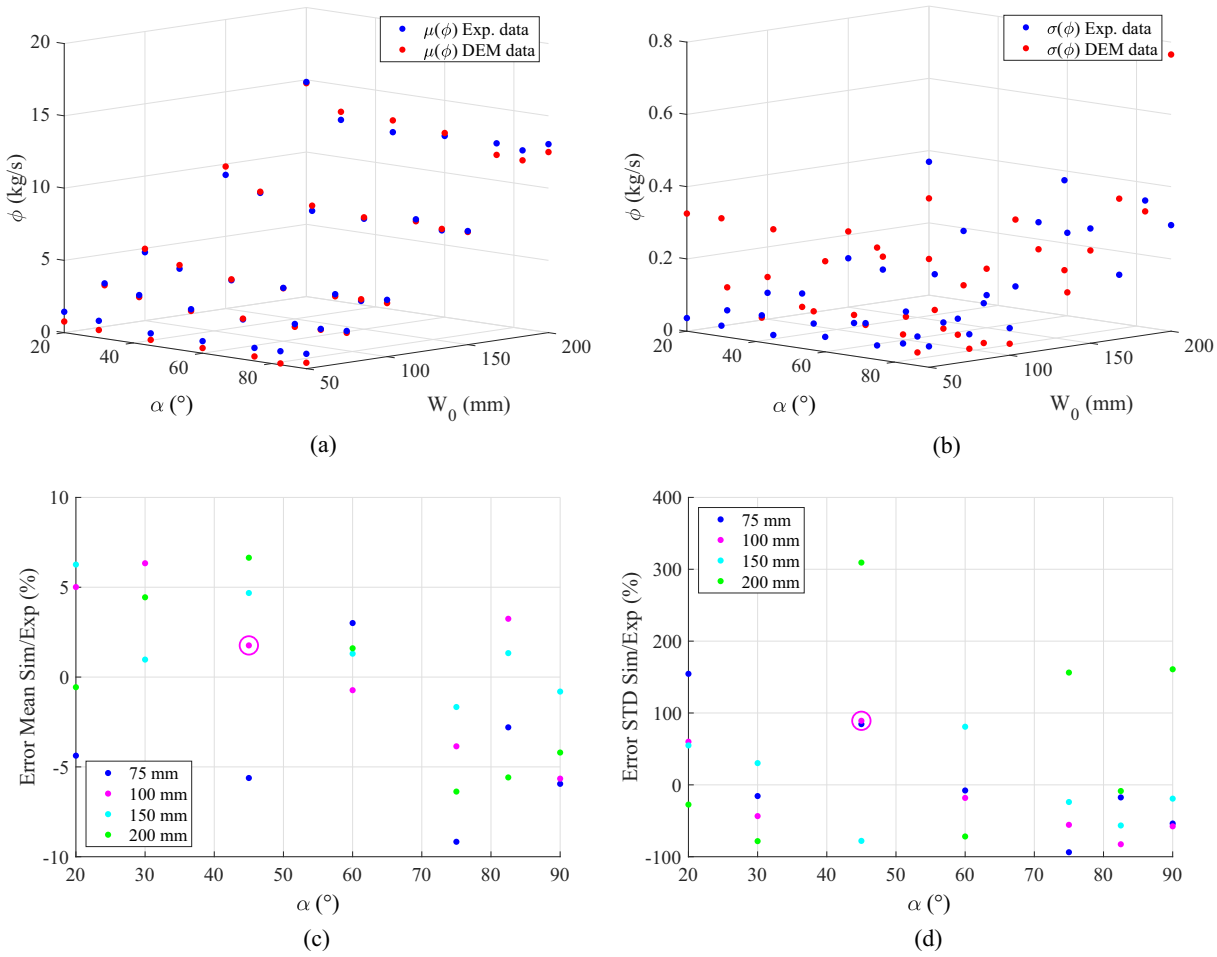

Fig. 11. DEM training data for metamodels (a) discharge rate (b) relative standard deviation discharge rate where the calibration results from [7] is shown by an additional circle.

References

[1] R.H. Byrd, J.C. Gilbert, J. Nocedal, A trust region method based on interior point techniques for nonlinear programming, Math. Prog. Series B 89 (1) (2000) 149–185, https://doi.org/10.1007/PL00011391.

[2] H. Cheng, T. Shuku, K. Thoeni, P. Tempone, S. Luding, V. Magnanimo, An iterative Bayesian filtering framework for fast and automated calibration of DEM models, Comput. Methods Appl. Mech. Eng. 350 (2019) 268–294.

[3] P.W. Cleary, DEM simulation of industrial particle flows: case studies of dragline excavators, mixing in tumblers and centrifugal mills, Powder Technol. 109 (1–3) (2000) 83–104, https://doi.org/10.1016/S0032-5910(99)00229-6.

[4] P.W. Cleary, DEM prediction of industrial and geophysical particle flows, Particuology 8 (2) (2010) 106–118, https://doi.org/10.1016/j.partic.2009.05.006.

[5] H.Q. Do, A.M. Aragón, D.L. Schott, A calibration framework for discrete element model parameters using genetic algorithms, Adv. Powder Technol. 29 (6) (2018) 1393–1403, https://doi.org/10.1016/j.apt.2018.03.001.

[6] M.P. Fransen, M. Langelaar, D. Schott, Application of DEM-based metamodels in bulk handling equipment design : methodology and DEM case study, Powder Technol. 393 (2021) 205–218, https://doi.org/10.1016/j.powtec.2021.07.048.

[7] M.P. Fransen, M. Langelaar, D. Schott, Including stochastics in metamodel-based DEM model calibration, Powder Technol. 406 (2022), 117400, https://doi.org/10.1016/j.powtec.2022.117400.

[8] S.W. Lommen, Virtual Prototyping of Grabs, TU Delft, 2016.

[9] R.T. Marler, J.S. Arora, Survey of Multi-Objective Optimization Methods for Engineering 395, 2004, pp. 369–395, https://doi.org/10.1007/s00158-003-0368-6.

[10] M.J. Mohajeri, W. de Kluijver, R.L.J. Helmons, C. van Rhee, D.L. Schott, A validated co-simulation of grab and moist iron ore cargo: replicating the cohesive and stress-history dependent behaviour of bulk solids, Adv. Powder Technol. 32 (4) (2021) 1157–1169, https://doi.org/10.1016/j.apt.2021.02.017.

[11] M.J. Mohajeri, H.Q. Do, D.L. Schott, DEM calibration of cohesive material in the ring shear test by applying a genetic algorithm framework, Adv. Powder Technol. 31 (5) (2020) 1838–1850, https://doi.org/10.1016/j.apt.2020.02.019.

[12] G.J. Park, T.H. Lee, K.H. Lee, K.H. Hwang, Robust design: an overview, AIAA J. 44 (1) (2006) 181–191, https://doi.org/10.2514/1.13639.

[13] C.E. Rasmussen, C.K.I. Williams, Gaussian Processes for Machine Learning Vol. 7, MIT Press, 2006. Issue 5.

[14] C. Richter, T. Rößler, G. Kunze, A. Katterfeld, F. Will, Development of a standard calibration procedure for the DEM parameters of cohesionless bulk materials – part II: efficient optimization-based calibration, Powder Technol. 360 (2020) 967–976, https://doi.org/10.1016/j.powtec.2019.10.052.

[15] C. Richter, F. Will, Introducing metamodel-based global calibration of material-specific simulation parameters for discrete element method, Minerals 11 (848) (2021).

[16] E.J. Rykiel, Testing ecological models: the meaning of validation, Ecol. Model. 90 (2) (1996) 229–244.

[17] D. Schott, J. Mohajeri, J. Jovanova, S. Lommen, W. de Kluijver, Design framework for DEM-supported prototyping of grabs including full-scale validation, J. Terrramech. 96 (2021) 29–43, https://doi.org/10.1016/j.jterra.2021.04.003.

[18] D. Schulze, Powders and Bulk Solids: Behavior, Characterization, Storage and Flow, 2008.

[19] G.G. Wang, S. Shan, Review of metamodeling techniques in support of engineering design optimization, J. Mech. Des. 129 (4) (2007) 370, https://doi.org/10.1115/1.2429697.